 https://doi.org/10.3311/PPee.37217


**Periodica Polytechnica Electrical Engineering and Computer Science**, 68(4), pp. 356–366, 2024

# Robust Intelligent Nonlinear Predictive Control Based on Artificial Neural Network for Optimizing PMSM Drive Performance

Amel Kasri[1]*, Kamel Ouari[1]

[1] Laboratoire de Technologie Industrielle et de l'Information, Faculté de Technologie, Université de Bejaia, 06000 Bejaia, Algeria
* Corresponding author, e-mail: amel.kasri@univ-bejaia.dz

Received: 27 April 2024, Accepted: 26 August 2024, Published online: 16 September 2024

**Abstract**

In the realm of high-performance motor drive systems, achieving stable and optimal motor operation is crucial, particularly in environments characterized by disturbances. The implementation of model predictive control (MPC) represents a strategic methodology. However, conventional predictive controllers frequently encounter challenges due to uncertainties regarding the motor's internal parameters and external load characteristics, subsequently impacting the effectiveness of the control algorithm. This paper proposes a new robust predictive control combined with an artificial neural network (RMPC-ANN) approach applied to a permanent magnet synchronous motor (PMSM) to tackle challenges posed by external perturbations and parameter variations. The development of the proposed robust predictive controller involves optimizing a novel finite horizon cost function based on Taylor series expansion, which incorporates dual integral action into the control law. Crucially, this approach eliminates the necessity for measuring and observing external perturbations and parameter uncertainties. Additionally, for attaining high-precision speed control, the speed loop regulation relies on a multi-layer feedforward ANN algorithm. A comprehensive comparison was conducted using MATLAB/SIMULINK, assessing performance across diverse operating conditions. To further substantiate the numerical simulation results, a hardware-in-the-loop (HIL) configuration is implemented on the OPAL-RT platform, demonstrating the robustness and efficiency of the proposed control strategy.

**Keywords**

artificial neural network, robust predictive control, permanent-magnet synchronous motor, intelligent speed controller

## 1 Introduction

The permanent magnet synchronous motor has emerged as a standout among AC motors due to its unique attributes including excellent efficacy, compact construction, and superior power density. As a result, in recent decades, the PMSM has been extensively employed across various high-precision machinery sectors [1]. Nevertheless, PMSM systems pose challenges due to their inherent nonlinearity and significant coupling. These systems often face uncertainties in modeling arising from parameter fluctuations and external disturbances typical in industrial environments [2].

In such settings, conventional linear control techniques encounter difficulties in attaining optimal control performance [3]. Hence, various advanced and effective control methods have been proposed, each depending on aspects like nonlinearity, optimization, and robustness methods, involving adaptive control [4], backstepping [5], sliding mode control [6], and intelligent approaches [7].

Model predictive control stands out as a highly effective advanced optimal control approach widely employed in various industrial settings [8]. Which utilizes a dynamic system model to anticipate future states, and then determines the forthcoming control actions by optimizing a predefined cost function at each sampling interval [9]. This method is adept at ensuring satisfactory system performance due to its inherent benefits, including straightforward modeling and effective handling of constraints for manipulated and controlled variables [10].

Throughout the process of control, fluctuations in PMSM temperature and saturation of the stator winding can result in mismatches in the parameters related to the inductance and stator resistance. Consequently, the issue

**Cite this article as:** Kasri, A., Ouari, K. "Robust Intelligent Nonlinear Predictive Control Based on Artificial Neural Network for Optimizing PMSM Drive Performance", Periodica Polytechnica Electrical Engineering and Computer Science, 68(4), pp. 356–366, 2024. https://doi.org/10.3311/PPee.37217

of model parameter mismatch can arise, resulting in prediction inaccuracies, which can negatively impact the system's performance [11]. Moreover, significant variations in load torque are common, necessitating a robust control system to maintain optimal response performance. As a result, challenges such as model parameter variations and external load disturbances have emerged, prompting an increasing number of researchers to concentrate on robust control techniques of MPC [12]. Various methods have been developed to enhance the robustness of MPC. A predictive functional controller, coupled with an extended state observer has been developed in [13] to achieve robust speed control. However, its effectiveness heavily relies on the precision of the parameters of the PMSM and demands a high sampling frequency for optimal performance. In [14], a load disturbance observer is implemented within the outer speed loop, to gauge the comprehensive disturbance. Simultaneously, real-time parameter observation is conducted within the inner current loop through stator flux and torque observers, exhibiting strong resilience against motor parameter uncertainties. In [15], a deadbeat current predictive control approach is introduced, aiming to suppress all parameter disturbances effectively. Despite its capability to reduce the sensitivity of PMSM driving parameters, this method necessitates the design of two observers, thereby raising the complexity level. There has been considerable focus on artificial neural networks in intelligent control systems. Drawing inspiration from the remarkable processing capabilities of the human brain, this technology holds promise in its ability to undergo training, learn from data, dynamically adjust, and improve over time [16]. In contrast to numerous conventional methodologies, ANNs do not necessitate explicit programming or in-depth system understanding [17]. Their aptitude to assimilate extensive datasets from diverse sensors and origins, and extract practical insights, distinguishes them.

In this paper, a highly robust controller based on an intelligent strategy is developed to efficiently address performance deterioration in controlling PMSM. The formulation of the robust predictive control law entails the optimization of a new cost function that incorporates an integral action. An outstanding feature of this innovative strategy lies in its inherent ability to bolster system resilience without requiring extensive knowledge of external perturbations or variations in system settings. Complementing this, a multi-layer feedforward artificial neural network algorithm is developed for the outer loop. The novel approach of robust model predictive control-based artificial neural network (RMPC-ANN) is being implemented for the inaugural time in PMSM control. The primary contributions of the suggested study are encapsulated as follows:

- The suggested controller ensures accurate set-point tracking despite variations in load torque and system parameters. Its design simplifies implementation by eliminating the need for a disturbance observer, making it effective and easy to use.
- The proposed controller ensures quick and responsive dynamic control while maintaining robustness against external disturbances and system uncertainties. Such enhancements contribute to heightened stability and optimized performance of the PMSM.

The remainder of this paper is structured as follows: The mathematical model of PMSM is elaborated in Section 2. Section 3 is devoted to thoroughly explaining the proposed RMPC-ANN control strategy. Section 4 is dedicated to the simulation results, as well as interpreting the obtained outcomes. Section 5 provides an analysis of the real-time results generated through the OPAL-RT platform. Lastly, conclusions are drawn in Section 6.

## 2 PMSM mathematical model

The stator voltage components of the PMSM depicted within the *d-q* referential frame are presented by [1]:

$$v_{sd} = R_s i_{sd} + L_d \frac{di_{sd}}{dt} - p\omega_r L_q i_{sq}, \tag{1}$$

$$v_{sq} = R_s i_{sq} + L_q \frac{di_{sq}}{dt} + p\omega_r L_d i_{sd} + p\omega_r \varphi_f . \tag{2}$$

The expressions for the current components along the *d-q* axis are formulated as follows:

$$\frac{di_{sd}}{dt} = -\frac{R_s}{L_d} i_{sd} + \frac{L_q}{L_d} p\omega_r i_{sq} + \frac{1}{L_d} v_{sd}, \tag{3}$$

$$\frac{di_{sq}}{dt} = -\frac{R_s}{L_q} i_{sq} - \frac{L_d}{L_q} p\omega_r i_{sd} - \frac{\varphi_f}{L_q} p\omega_r + \frac{1}{L_q} v_{sq}. \tag{4}$$

The electromagnetic torque can be determined by:

$$T_{em} = \frac{3}{2} p\left(\varphi_f i_{sq} + \left(L_d + L_q\right) i_{sd} i_{sq}\right). \tag{5}$$

The PMSM's mechanical equation can be defined as follows:

$$\frac{d\omega_r}{dt} = \frac{1}{J}\left(T_{em} - f_r \omega_r - T_L\right) \tag{6}$$

with stator voltages $v_{sd}$ and $v_{sq}$, stator currents $i_{sd}$ and $i_{sq}$ stator resistance $R_s$, the mechanical rotor speed $\omega_r$, direct inductance $L_d$, longitudinal inductance $L_q$, permanent magnet flux $\varphi_f$, the number of pole pairs $p$, moment

of inertia $J$, friction coefficient $f_r$, and load torque $T_L$. By selecting the state variable vector $x(t)=\begin{bmatrix} i_{sd} & i_{sq} & \omega_r \end{bmatrix}$ and the control input vector $u(t)=\begin{bmatrix} v_{sd} & v_{sq} \end{bmatrix}$, the representation of the PMSM model is expressed in the nonlinear matrix form by:

$$\begin{cases} \dot{x}(t)=A(x)+B\cdot u(t) \\ y_i(t)=h_i(x) \end{cases} \tag{7}$$

with

$$A=\begin{bmatrix} -\dfrac{R_s}{L_d}i_{sd}+\dfrac{L_q}{L_d}p\omega_r i_{sq} \\ -\dfrac{R_s}{L_q}i_{sq}-p\dfrac{L_d}{L_q}\omega_r i_{sd}-\dfrac{\varphi_f p\omega_r}{L_q} \\ \dfrac{1}{J}\left(T_{em}-f_r\omega_r-T_L\right) \end{bmatrix};B=\begin{bmatrix} \dfrac{1}{L_d} & 0 \\ 0 & \dfrac{1}{L_q} \\ 0 & 0 \end{bmatrix}.$$

## 3 Design of the suggested robust control strategy

In this segment, a new robust predictive control combined with an artificial neural network algorithm is devised to control PMSM. A diagram illustrating the control structure is depicted in Fig. 1. The implemented control architecture comprises two distinct control loops. The inner loop is constructed utilizing a novel robust predictive control strategy, specifically designed to regulate torque $T_{em}$ and current $i_{sd}$ to accurately follow desired commands. The outer control loop incorporates a multi-layer feedforward artificial neural network speed controller, aiming to regulate the speed to its desired value.

### 3.1 Traditional model predictive control

Model predictive control represents an advanced approach designed to enhance motor performance by accounting for system constraints and dynamics [18]. Fundamentally,

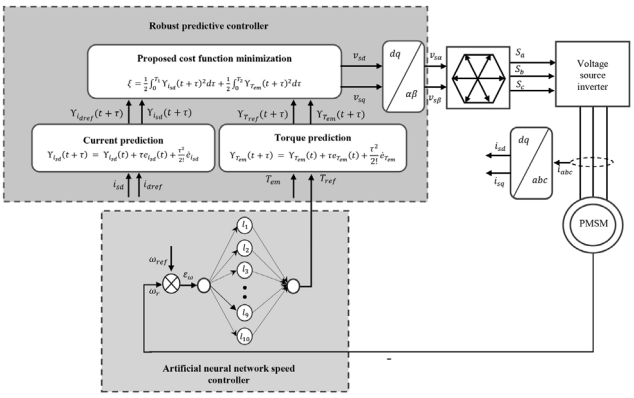


**Fig. 1** Proposed robust model predictive neural network control system applied to a PMSM

MPC constructs a predictive model of the PMSM to anticipate its behavior within a specific time frame [19]. These predictions are subsequently employed to determine the most suitable control action, by solving an optimization problem while ensuring adherence to predefined cost functions, defined by [20]:

$$\xi=\frac{1}{2}\int_0^{T_1}e_1\left(t+\tau\right)^2 d\tau+\frac{1}{2}\int_0^{T_2}e_2\left(t+\tau\right)^2 d\tau \tag{8}$$

with

$$e_1\left(t+\tau\right)=y_{1ref}\left(t+\tau\right)-y_1\left(t+\tau\right),$$

$$e_2\left(t+\tau\right)=y_{2ref}\left(t+\tau\right)-y_2\left(t+\tau\right).$$

Where $y_{1,2}(t+\tau)$ represents the anticipated outputs, $y_{1ref,2ref}(t+\tau)$ denotes the anticipated references trajectory, and $T_{1,2}>0$ represents the prediction horizon, the control outputs consist of the electromagnetic torque $T_{em}$ and the d-axis current $i_{sd}$ defined as follows:

$$\begin{bmatrix} y_1(t) \\ y_2(t) \end{bmatrix}=\begin{bmatrix} i_{sd} \\ T_{em} \end{bmatrix}. \tag{9}$$

To address the nonlinear optimization problem of Eq. (8), an approach involves expanding the anticipated output and reference trajectory using an $\rho_i^{th}$ order Taylor series through the application of the Lie derivative, the following results are derived [21]:

$$y_i\left(t+\tau\right)=h_i\left(x\right)+\sum_{l=1}^{\rho_i}\frac{\tau^l}{l!}L_A^l h_i\left(x\right)+\psi\left(x\right)u\left(t\right) \tag{10}$$

with

$$\psi\left(x\right)=\frac{\tau^l}{\rho_i!}L_B L_A^{(\rho_i-1)}h_i\left(x\right).$$

Lie derivatives of $h(x)$ concerning $A(x)$ are defined recursively as follows:

$$\begin{cases} L_A h_i\left(x\right)=\dfrac{\partial h_i}{\partial x}A\left(x\right) \\ L_A^l h_i\left(x\right)=L_A\left(L_A^{l-1}h_i\left(x\right)\right) \\ L_B L_A h_j\left(x\right)=\dfrac{\partial L_A h_j}{\partial x}B\left(x\right) \end{cases}. \tag{11}$$

Utilizing predictive control through Taylor series expansion facilitates accurate control of nonlinearities, ensuring optimal trajectory tracking performance, provided that the engine parameters remain unchanged. Nevertheless, MPC poses certain hurdles, it necessitates a precise dynamic representation of the motor, a task that could prove

challenging in real-world scenarios [16]. It entirely misses the concept of robustness when confronted with external parameter disruptions or uncertainties.

### 3.2 Proposed robust predictive control based on a new cost function

To address the drawbacks associated with conventional MPC, a new cost function is proposed, incorporating integral action into the controller's minimization process. The suggested cost function enables the development of a general form for robust predictive control, ensuring the rejection of any external disturbances. This can be accomplished by modifying the traditional cost function in Eq. (8) to:

$$\xi = \frac{1}{2}\int_0^{T_1} \Upsilon_{i_{sd}}\left(t+\tau\right)^2 d\tau + \frac{1}{2}\int_0^{T_2} \Upsilon_{T_{em}}\left(t+\tau\right)^2 d\tau\,, \tag{12}$$

where

$$\Upsilon_{i_{sd}}\left(t\right) = \int_0^t e_{i_{sd}}\left(\tau\right)d\tau = \int_0^t \left[i_{dref}\left(\tau\right) - i_{sd}\left(\tau\right)\right]d\tau\,,$$

$$\Upsilon_{T_{em}}\left(t\right) = \int_0^t e_{T_{em}}\left(\tau\right)d\tau = \int_0^t \left[T_{ref}\left(\tau\right) - T_{em}\left(\tau\right)\right]d\tau\,.$$

Emphasizing the significance of the minimization criterion operating over a future horizon, it becomes crucial to construct a prediction model for computing the integrals of forthcoming output errors. The anticipated term $\Upsilon(t + \tau)$ is determined utilizing the Taylor series expansion. In this case, the differentiation of the error integral is iterated $(\rho_i + 1)^{\text{th}}$ times to integrate the $u(t)$ command into the prediction model, thus yielding to:

$$\Upsilon_i\left(t+\tau\right) = \Upsilon_i\left(t\right) + \tau e_i\left(t\right) + \frac{\tau^2}{2!}\dot{e}_i\left(t\right) + \psi\left(x\right)u\left(t\right) \tag{13}$$

with

$$\psi\left(x\right) = \frac{\tau^{\rho_i+1}}{\left(\rho_i+1\right)!} e_i\left(t\right)^{(\rho_i)} L_B L_A^{(\rho_i-1)} h_i\left(x\right).$$

The $u_d(t)$ and $u_q(t)$ commands are observed within the first derivative of $y_1(t)$ and $y_2(t)$, respectively. Consequently, the relative degrees $\rho_{1,2} = 1$, this yields the following outcome:

$$\Upsilon_{i_{sd}}\left(t+\tau\right) = \Upsilon_{i_{sd}}\left(t\right) + \tau e_{i_{sd}}\left(t\right) + \frac{\tau^2}{2!}\dot{e}_{i_{sd}}\,, \tag{14}$$

$$\Upsilon_{T_{em}}\left(t+\tau\right) = \Upsilon_{T_{em}}\left(t\right) + \tau e_{T_{em}}\left(t\right) + \frac{\tau^2}{2!}\dot{e}_{T_{em}} \tag{15}$$

with

$$\dot{e}_{i_{sd}} = \dot{i}_{dref}\left(t\right) - L_A h_1\left(x\right) - \Gamma_1\left(x\right)u_d\left(t\right),$$

$$\dot{e}_{T_{em}} = \dot{T}_{ref}\left(t\right) - L_A h_2\left(x\right) - \Gamma_2\left(x\right)u_q\left(t\right).$$

By incorporating Eqs. (14) and (15) into the novel cost function Eq. (12), the following is given:

$$\xi = \frac{1}{2}[\Phi]^T \int_0^{\tau_r} \left(\Pi\left(\tau\right)^T \Pi\left(\tau\right)\right)d\tau\,[\Phi]\,, \tag{16}$$

where

$$\Pi\left(\tau\right) = \begin{bmatrix} 1 & 0 & \tau & 0 & \dfrac{\tau^2}{2} & 0 \\ 0 & 1 & 0 & \tau & 0 & \dfrac{\tau^2}{2} \end{bmatrix},$$

$$\Phi = \begin{bmatrix} \Upsilon_{i_{sd}}\left(t\right) \\ \Upsilon_{T_{em}} \\ i_{dref}\left(\tau\right) - i_{sd}\left(\tau\right) \\ T_{ref}\left(\tau\right) - T_{em}\left(\tau\right) \\ \dot{i}_{dref}\left(t\right) - L_A h_1\left(x\right) - \Gamma_1\left(x\right)u_d\left(t\right) \\ \dot{T}_{ref}\left(t\right) - L_A h_2\left(x\right) - \Gamma_2\left(x\right)u_q\left(t\right) \end{bmatrix}.$$

The required condition for optimal control is defined by:

$$\frac{d\xi}{dt} = 0\,. \tag{17}$$

This amounts to solving the following system of equations:

$$\frac{d\xi}{dt} = \frac{d}{dt}\left[\frac{1}{2}[\Phi]^T \int_0^{\tau_r} \left(\Pi\left(\tau\right)^T \Pi\left(\tau\right)\right)d\tau\,[\Phi]\right] = 0\,. \tag{18}$$

Assuming the condition in Eq. (17), the optimal input for control shall then be given as:

$$u = -\Gamma^{-1}\begin{bmatrix} \delta_0^1 \Upsilon_{i_{sd}} + \sum_{i=1}^{2} \delta_i^1 \left(\dot{i}_{dref}{}^{i-1} - L_A{}^{i-1} h_1\right) \\ \delta_0^2 \Upsilon_{T_{em}} + \sum_{i=1}^{2} \delta_i^2 \left(T_{ref}{}^{i-1} - L_A{}^{i-1} h_2\right) \end{bmatrix} \tag{19}$$

with

$$\begin{cases} \delta_0^1 = \dfrac{10}{3T_1^2} \\ \delta_1^1 = \dfrac{5}{2T_1} \\ \delta_2^1 = 1 \end{cases}; \begin{cases} \delta_0^2 = \dfrac{10}{3T_2^2} \\ \delta_1^2 = \dfrac{5}{2T_2} \\ \delta_2^2 = 1 \end{cases}.$$

The decoupling matrix is defined as follows:

$$\Gamma(x)=\begin{bmatrix} \dfrac{1}{L_d} & 0 \\ \dfrac{3p}{2L_d}\left(L_d-L_q\right)i_{sq} & \dfrac{3p}{2L_q}\left(\left(L_d-L_q\right)i_{sd}+\varphi_f\right) \end{bmatrix}. \quad (20)$$

To guarantee that the matrix $\Gamma^{-1}(x)$ can be inverted, it is sufficient for condition $(L_d - L_q)i_{sd} + \varphi_f \neq 0$ to be met.

### 3.3 Artificial neural network speed controller

Artificial neural networks serve as mathematical representations that draw inspiration from the intricate workings of the human brain [22]. It consists of multiple nonlinear computational components, known as neurons, operating concurrently and interconnected through forces represented by numerical values termed weights [23]. The neuron forms the foundation of artificial neural networks, comprising summation and activation functions, as depicted in Fig. 2 [24]. In this approach, ANN is employed to provide the torque reference $T_{ref}$, the variable $\varepsilon_\omega$ denotes the error between the desired speed and the actual speed.

#### 3.3.1 Dataset collection

The first stage in designing the ANN involves acquiring the necessary datasets. In this context, the datasets were obtained from the simulation results, specifically capturing the input and output values of the speed regulator (PI) used in the system. The learning base must encompass a thorough understanding of all pertinent aspects related to the diverse operational modes of the variable speed drive system. The data is randomly split into three separate subsets designated for training, validation, and testing as described below:

- 70% of the data is allocated for training.
- 15% is designated for network validation
- 15% is utilized for testing the learning process.

In the subsequent phase, we initiated the process by configuring the neural network controller using MATLAB's graphical user interface, known as "nntool" (released in MATLAB R2021b) [25]. We selected a configuration that has a single hidden layer and a decreased number of neurons. While assessing the network's performance, we gradually augment the number of neurons until reaching the desired level of effectiveness. Tangent-sigmoid functions were employed as activation functions for the neurons in the hidden layer, while linear activation functions were applied for the network output.

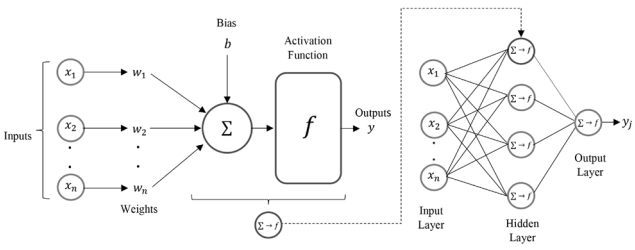


**Fig. 2** From a solitary perceptron to an artificial neural network

#### 3.3.2 Performance evaluation

To evaluate the effectiveness of the developed network model, this study utilized the Mean Squared Error (MSE) as a key performance metric. MSE measures the average squared differences between the outputs generated by the ANN and the actual target values. The optimal ANN controller is identified by achieving the lowest MSE during simulation, indicating a closer match between the model's predictions and the target data. During the training process, the weights are iteratively adjusted using the Levenberg-Marquardt backpropagation algorithm. This adjustment continues through each iteration (epoch) until the error levels reach an acceptable threshold. If the error fails to converge adequately, adjustments are made to the neural network architecture by modifying the number of neurons in the hidden layer or by altering the number of hidden layers. Based on the established MSE criteria, we concluded that the most effective configuration for the controller is a Multi-Layer Perceptron Feedforward network with 10 neurons in the hidden layer. Details regarding the neural network parameters can be found in Table 1. The ANN speed controller quickly aligns the trained results with the target values, achieving a stable mean squared error (MSE) of $2.81 \cdot 10^{-7}$ after 436 epochs, as illustrated in Fig. 3.

## 4 Simulation results and discussions

To assess the effectiveness of the newly developed robust model predictive artificial neural network control strategy (RMPC-ANN), a simulation model of a PMSM was

**Table 1** The optimal proposed ANN configurations

| Parameters of ANN | ANN speed controller |
|---|---|
| Neural network | Two-layer feedforward network |
| Number of hidden layer nodes | 10 |
| Number of neurons in the input layer | 1 |
| Number of neurons in hidden layer 2 | 1 |
| Number of neurons in output layer | 1 |
| Activation function | Tansig |
| Adaption learning function | Trainlm |

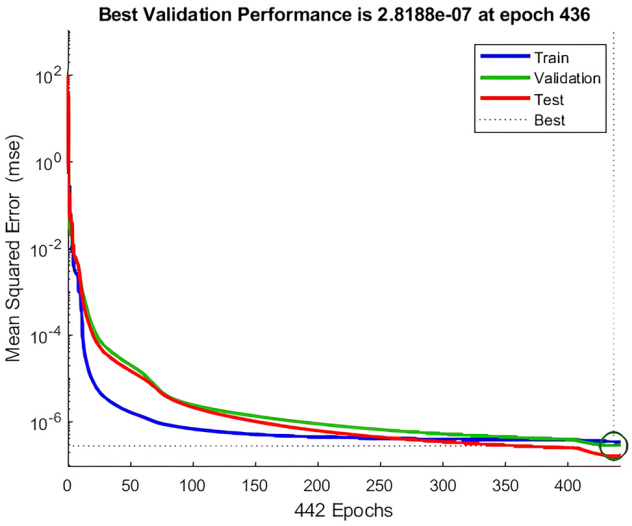


**Fig. 3** Training performance based on MSE

created using Matlab/Simulink [25]. The specifications of the PMSM are outlined in Table 2, the prediction $T_1$ and $T_2$ are both configured to 0.5 ms alongside a sampling time of $10^{-5}$ s. A comparison is drawn between the suggested approach and two conventional methods, namely model predictive control strategy (MPC) and proportional integral controller (PI), regarding their ability to track references, reject disturbances, maintain robustness, ensure current quality, and minimize ripple values. To constrain the control effort, the reference speed signal undergoes filtering via a second-order linear filter described as follows:

$$H(s)=\frac{\omega_n^{\,2}}{s^2+2\zeta\omega_n s+\omega_n^{\,2}};\ \text{with: } \omega_n=10,\ \zeta=1. \tag{21}$$

### 4.1 Performance evaluation under load torque disturbances

In the initial test, the starting reference speed is set at 100 rad/s, followed by a subsequent setting of –100 rad/s, to assess the PMSM's performance in both forward and reverse rotations. During operation according to the speed characteristic, the motor experiences a sudden change in load torque, with 5 Nm applied at $t$ = 2 s then 13 Nm at $t$ = 5 s, while operating with fixed parameters.

**Table 2** Characteristics of PMSM

| Parameter | Value |
|---|---|
| Rated current | 31 A |
| Rated voltage | 310 V |
| Nominal torque | 22 Nm |
| Direct inductance | 0.8524 mH |
| Quadratic inductance | 0.9515 mH |
| Number of pole pairs | 4 |
| Stator resistance | 0.17377 Ω |
| Permanent magnet flux | 0.1112 Wb |
| Friction coefficient | 0.0085 N·m·s/rad |
| Moment of inertia | 0.0048 kg·m² |

Fig. 4 displays the simulation results illustrating the speed trajectory tracking performance. It's evident that the proposed control effectively mitigates the impact of load torque fluctuations on the system's speed response. Notably, the speed signal exhibits an exceptionally rapid response time, effortlessly retaining its reference point with minimal latency. Fig. 5 illustrates the speed trajectory tracking error, comparing traditional approaches with the proposed control method. The speed error plot demonstrates favorable outcomes with the proposed controller, with overshoot/undershoot levels consistently below 0.0004 pu for all speed adjustments with no steady-state error.

Fig. 6 depicts the simulation results for the developed electromagnetic torque across different load torque conditions. The findings underscore several significant enhancements, the implementation of the RMPC-ANN yields swift torque response with minimal overshoot. It effectively

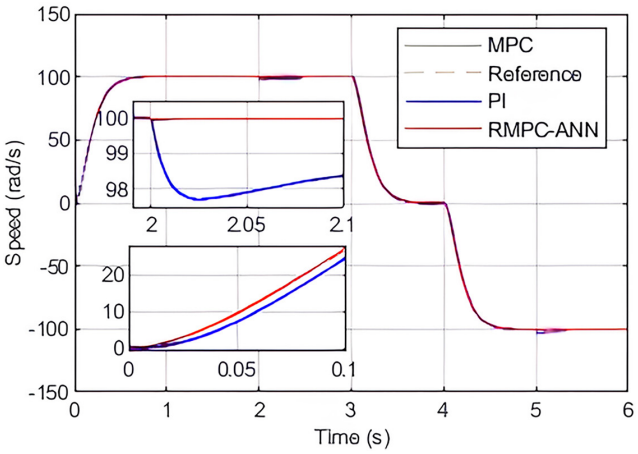


**Fig. 4** Speed trajectory tracking response

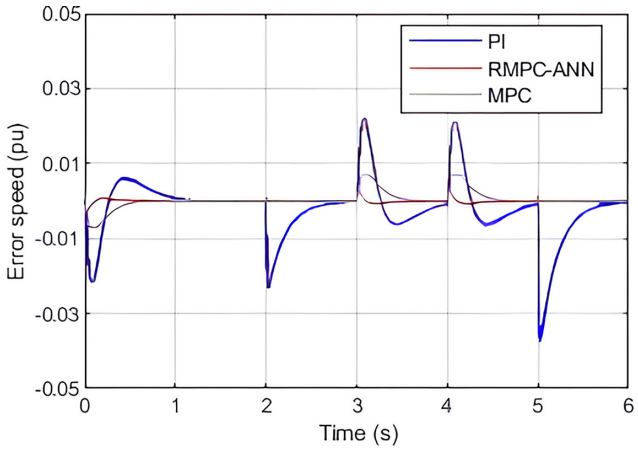


**Fig. 5** Speed trajectory tracking error response

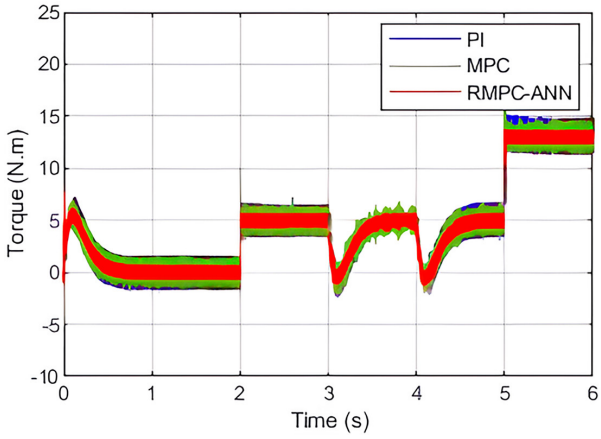


**Fig. 6** Electromagnetic torque response

adapts to step inputs in the load torque, exhibiting negligible response delay and substantially reducing torque ripple across most operational scenarios. As shown in the zoomed-in section of torque response in Fig. 7, there's an observed reduction of approximately 66.66%, indicating that the implementation of the RMPC-ANN approach significantly contributes to mitigating unwanted torque ripple.

Fig. 8 illustrates the inverter current $i_{sa}$ of the three control methods, furthermore, a zoomed-in section is provided in Fig. 9. The inverter current exhibits sinusoidal behavior, with its magnitude directly linked to the torque generated by the motor. Notably, the RMPC-ANN system demonstrates a substantially reduced current ripple, and the THD remains remarkably low, registering at 3.37%. This performance surpasses that achieved by both the traditional MPC strategy (4.69%) and the PI (7.39%). The RMPC-ANN strategy achieves a reduction in THD by approximately 54.4%. Consequently, the peak current is lowered, enhancing the quality of power supplied to the motor.

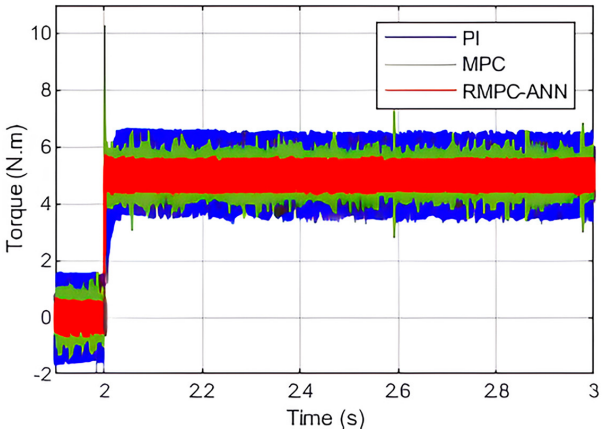


**Fig. 7** Zoomed-in section of electromagnetic torque response

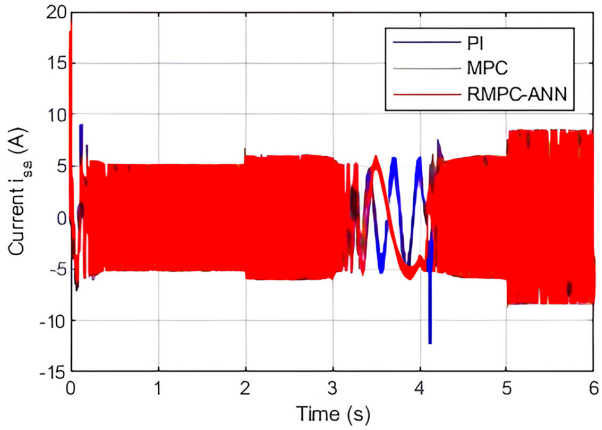


**Fig. 8** Stator current $i_{sa}$

### 4.2 Performance evaluation under parameters uncertainties

In the second test, the plant model encountered uncertainties and fluctuations in parameters. For each simulation run, a single parameter was altered starting at $t = 1$ s, while a set point step of 100 rads/s was implemented for each test. The robustness tests comprise introducing uncertainty to the electrical and mechanical system parameters:

- The stator resistance $R_s$ by +30%
- The moment of inertia $J$ by +20%.

Figs. 10 and 11 depict the simulation outcomes, showcasing the speed trajectory tracking capabilities of the proposed RMPC-ANN in comparison to conventional control approaches, under uncertainties in electrical and mechanical parameters. Both the RMPC-ANN and MPC control algorithms exhibit adept tracking of the speed desired trajectory, demonstrating swift responses and effective disturbance rejection, unlike the PI controller. Nevertheless, the suggested controller showcases improved stability features, characterized by a resilient response and skilled disturbance rejection abilities. Figs. 12 and 13 illustrate the speed trajectory tracking error, the finding show that the suggested control method displays notably reduced speed

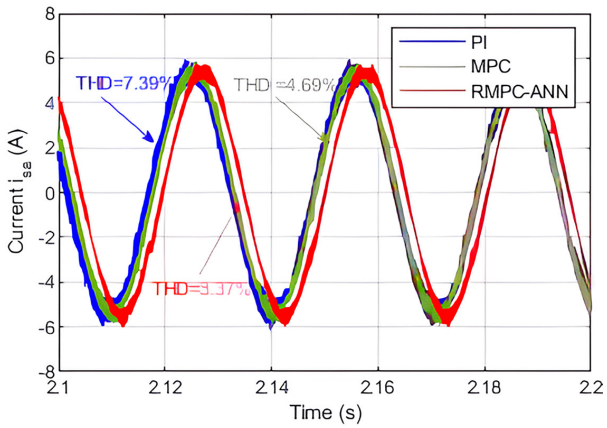


**Fig. 9** Zoomed-in section of stator current $i_{sa}$

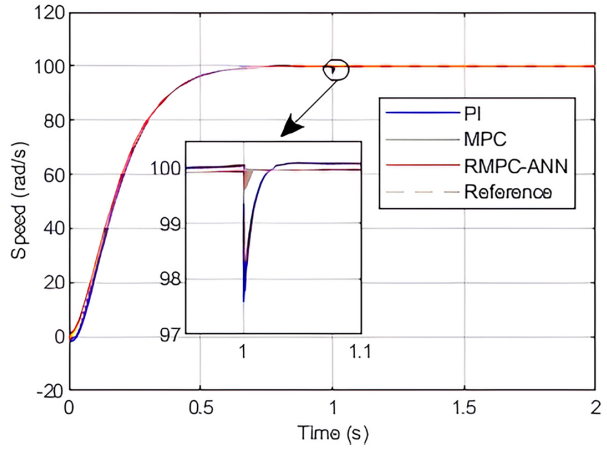


**Fig. 10** Speed trajectory tracking under variation of 30% $R_s$

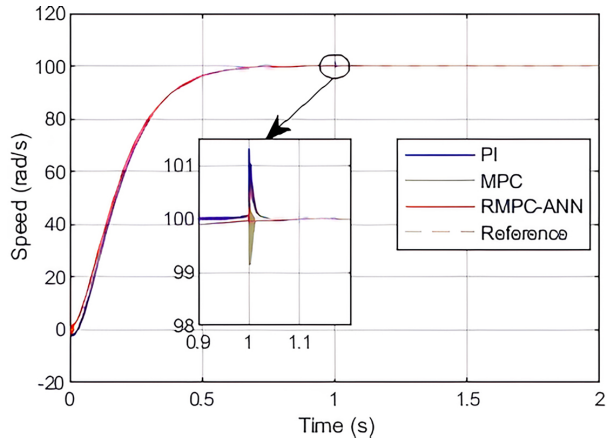


**Fig. 11** Speed trajectory tracking under variation of 20% $J$

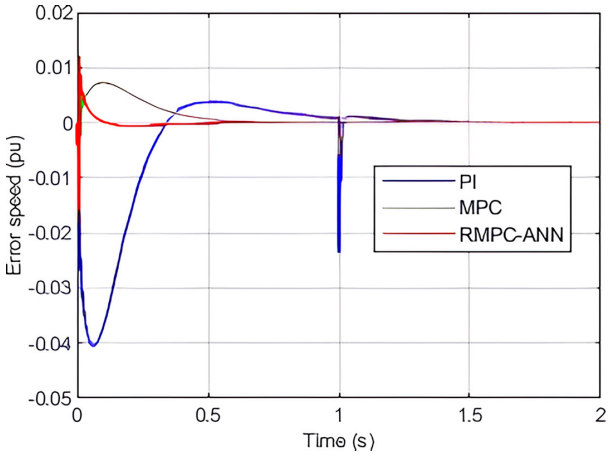


**Fig. 12** Speed tracking error under variation of 30% $R_s$

tracking errors compared to the two traditional approaches. Additionally, the error diminishes swiftly toward zero. Figs. 14 and 15 illustrate the simulation outcomes for the generated electromagnetic torque, providing a comparison of performance among the PI and MPC controllers, and the RMPC-ANN control under uncertainties in electrical and mechanical parameters. To evaluate the effectiveness of the controlled responses, two widely utilized metrics integral

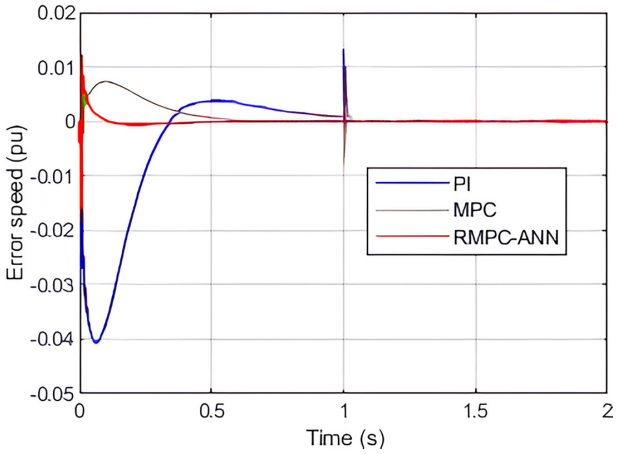


**Fig. 13** Speed tracking error under variation of 20% $J$

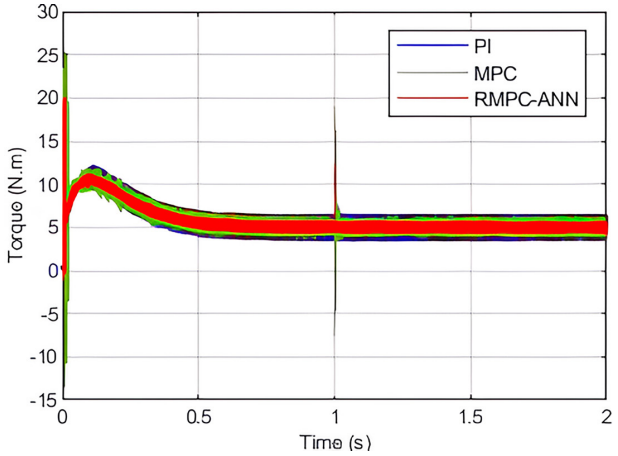


**Fig. 14** Electromagnetic torque responses under variation of 30% $R_s$

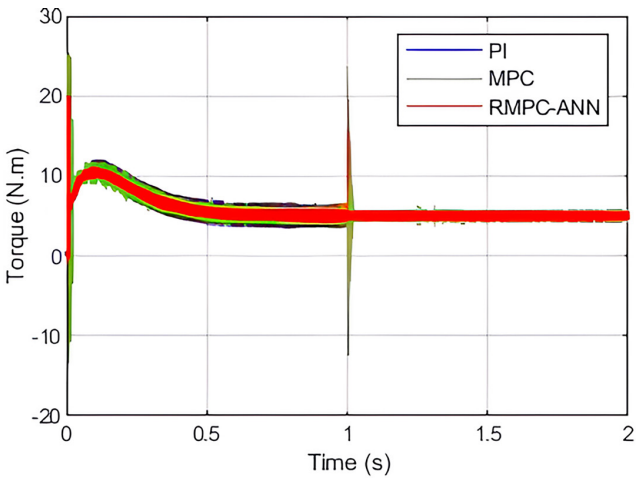


**Fig. 15** Electromagnetic torque responses variation of 20% $J$

time-weighted absolute error (ITAE) and integral squared error (ISE), were utilized in combination with various control methods. The results in Figs. 16 and 17 demonstrate the effectiveness of RMPC-ANN over classic techniques. Table 3 presents a summary of the test outcomes, highlighting the notable enhancements achieved by the RMPC-ANN technique across various parameters.

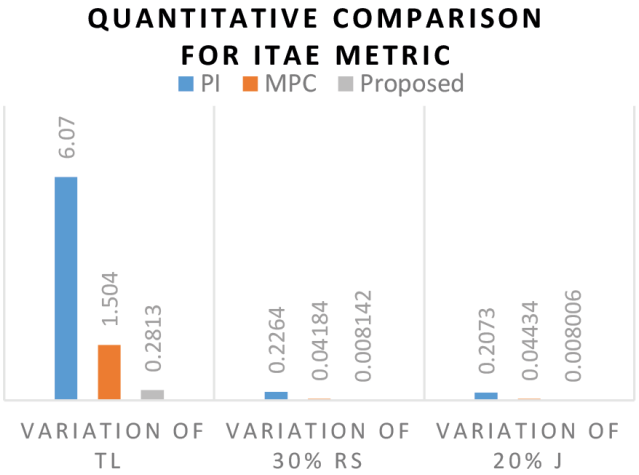


**Fig. 16** The quantitative comparison for the ITAE metric

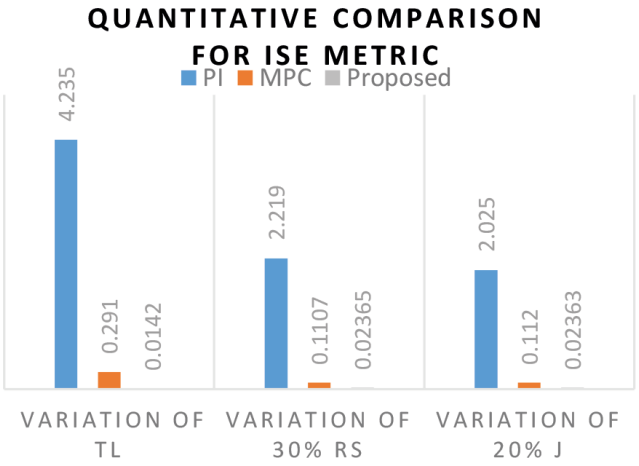


**Fig. 17** The quantitative comparison for the ISE metric

## 5 Experimental results

The OPAL-RT setup features an RT-Lab Hardware-in-the-Loop (HIL) simulator based on the OP-4510 board. As shown in Fig. 18, the real-time simulation bench comprises several key components:

1. MATLAB/Simulink software integrated with the RT-Lab platform,
2. a host PC,
3. the OPAL-RT 4510, and
4. a digital oscilloscope.

The OPAL-RT system is a sophisticated simulation platform compatible with Kintex-7 FPGA systems. It operates on the Linux OS and is driven by four active Intel Xeon E5 processor cores, each clocked at 3.2 GHz.

The experimental results under load torque disturbances and parameter variation are illustrated in Figs 19–22. Notably, the outcomes obtained from the real-time simulator, RT-LAB, closely align with the results predicted by the simulation.

Fig. 19 illustrates that the proposed controller ensures accurate reference tracking by precisely regulating motor speed, offering a rapid dynamic response with the error converging to zero. Moreover, the RMPC-ANN approach demonstrates superior performance in minimizing overshoot during load torque variations. Fig. 20 depicts the real-time electromagnetic torque responses of the PMSM, the RMPC-ANN controller greatly diminishes electromagnetic torque ripple.

To evaluate the proposed method's effectiveness under parameter variation, Figs. 21 and 22 present experimental results comparing the traditional PI controller with the new approach. $R_s$ is the parameter being tested. The real-time tests assess how the system responds to parameter changes. Fig. 21 shows that the speed closely tracks the reference trajectory. Even in the presence of parameter variation, the control system effectively eliminates steady-state errors, ensuring precise tracking. Fig. 22 indicates that the RMPC-ANN controller's error rapidly converges to zero unlike the classical controller, which experiences increasing error with changes in $R_s$. These results demonstrate the effectiveness of the proposed control strategy.

## 6 Conclusion

This study introduces a novel robust model predictive control based on an artificial neural network strategy for controlling PMSM. A significant contribution of this research involves introducing an innovative cost function for robust predictive control, which includes incorporating integral action within

**Table 3** Comparative analysis between RMPC-ANN, MPC, and PI strategies

| Metric | PI | MPC | Proposed RMPC-ANN |
|---|---|---|---|
| Dynamic torque response | Fast | Fast | Very fast |
| Adaptability to variations | Limited | Limited | High |
| Torque ripple | High | Medium | Very low |
| Reference tracking precision | Moderate | High | High |
| Sensitivity to disturbances | High | Low | Very low |
| Response to model changes | Sensitive | Sensitive | Robust |
| Current THD | High | Medium | Low |

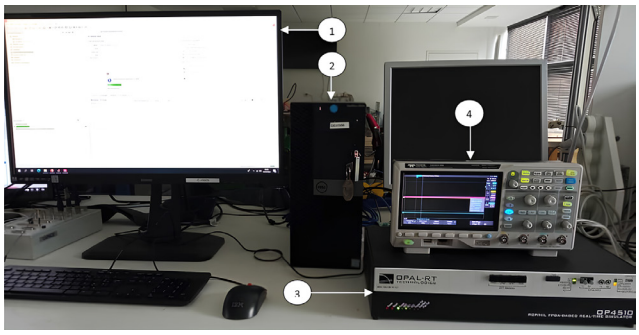


**Fig. 18** Real-time experimental setup

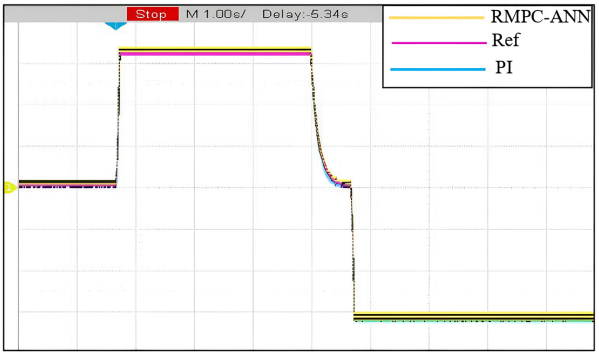


**Fig. 19** Real-time response of speed under $T_L$ variations


**Fig. 20** Real-time response of torque under $T_L$ variations

the control loop, it is complemented by a multi-layer artificial neural network speed controller to enhance the overall effectiveness. The performance of the RMPC-ANN


**Fig. 21** Real-time response of speed under variation of $R_s$

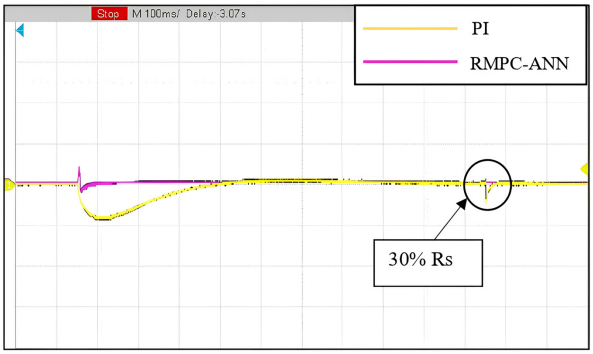


**Fig. 22** Real-time response of speed error under variation of $R_s$

strategy is analyzed in comparison alongside two other control methods. Multiple goals are accomplished, and the primary findings can be summarized as follows: improved tracking accuracy, heightened control precision, faster transient response, better disturbance rejection, and increased robustness to uncertainties on the motor's internal parameters and external load characteristics. Furthermore, there has been a 54.40% reduction in current ripple and significantly diminished fluctuations in electromagnetic torque, marking a 66.66% advancement over the traditional method. The outcomes of this investigation emphasize the superiority of the RMPC-ANN proposed in enhancing the performance of PMSM drives compared to traditional control techniques. The proposed control approach was validated using a hardware-in-the-loop setup with the OPAL-RT platform.

## References

[1] Karboua, D., Toual, B., Kouzou, A., Douara, B. O., Mebkhouta, T., Bendenidina, A. N. "High-order supper-twisting based terminal sliding mode control applied on three phases permanent synchronous machine", Periodica Polytechnica Electrical Engineering and Computer Science, 67(1), pp. 40–50, 2023. https://doi.org/10.3311/PPee.21026

[2] Zhao, X., Wang, C., Duan, W., Jiang, J. "Research on sensorless control system of low speed and high power PMSM based on improved high-frequency signal injection", Energy Reports, 7, pp. 499–504, 2021. https://doi.org/10.1016/j.egyr.2021.01.066

[3] Xu, B., Zhang, L., Ji, W. "Improved non-singular fast terminal sliding mode control with disturbance observer for PMSM drives", IEEE Transactions on Transportation Electrification, 7(4), pp. 2753–2762, 2021. https://doi.org/10.1109/TTE.2021.3083925

[4] Szczepanski, R., Tarczewski, T., Grzesiak, L. M. "Adaptive state feedback speed controller for PMSM based on artificial bee colony algorithm", Applied Soft Computing, 83, 105644, 2019. https://doi.org/10.1016/j.asoc.2019.105644

[5] Saidi, Y., Mezouar, A., Miloud, Y., Benmahdjoub, M. A., Brahmi, B., Kerrouche, K. D. E. "Lyapunov function based flux and speed observer using advanced non-linear backstepping DVC for PWM-rectifier connected wind-turbine-driven PM generator", 65(3), pp. 174–185, 2021.
https://doi.org/10.3311/PPee.17005

[6] Wu, L., Liu, J., Vazquez, S., Mazumder, S. K. "Sliding mode control in power converters and drives: a review", IEEE/CAA Journal of Automatica Sinica, 9(3), pp. 392–406, 2022.
https://doi.org/10.1109/JAS.2021.1004380

[7] Tan, L. N., Cong, T. P., Cong, D. P. "Neural network observers and sensorless robust optimal control for partially unknown PMSM with disturbances and saturating voltages", IEEE Transactions on Power Electronics, 36(10), pp. 12045–12056, 2021.
https://doi.org/10.1109/TPEL.2021.3071465

[8] Babqi, A. J. "A novel model predictive control for stability improvement of small scaled zero-inertia multiple DGs micro-grid", Periodica Polytechnica Electrical Engineering and Computer Science, 66(2), pp. 163–173, 2022.
https://doi.org/10.3311/PPee.19232

[9] Falkowski, P., Sikorski, A. "Finite control set model predictive control for grid-connected AC-DC converters with LCL filter", IEEE Transactions on Industrial Electronics, 65(4), pp. 2844–2852, 2018.
https://doi.org/10.1109/TIE.2017.2750627

[10] Meng, Q., Bao, G. "A novel low-complexity cascaded model predictive control method for PMSM", Actuators, 12(9), 349, 2023.
https://doi.org/10.3390/act12090349

[11] Zhang, S., Dai, L., Xia, Y. "Adaptive MPC for constrained systems with parameter uncertainty and additive disturbance", IET Control Theory amd Applications, 13(15), pp. 2500–2506, 2019.

[12] Niu, S., Luo, Y., Fu, W., Zhang, X. "Robust model predictive control for a three-phase PMSM motor with improved control precision", IEEE Transactions on Industrial Electronics, 68(1), pp. 838–849, 2021.
https://doi.org/10.1109/TIE.2020.3013753

[13] Wang, Y., Yu, H., Che, Z., Wang, Y., Zeng, C. "Extended state observer-based predictive speed control for permanent magnet linear synchronous motor", Processes, 7(9), 618, 2019.
https://doi.org/10.3390/pr7090618

[14] Wang, J., Wang, F., Zhang, Z., Li, S., Rodriguez, J. "Design and implementation of disturbance compensation-based enhanced robust finite control set predictive torque control for induction motor systems", IEEE Transactions on Industrial Informatics, 13(5), pp. 2645–2656, 2017.
https://doi.org/10.1109/TII.2017.2679283

[15] Gong, Z., Zhang, C., Ba, X., Guo, Y. "Improved deadbeat predictive current control of permanent magnet synchronous motor using a novel stator current and disturbance observer", IEEE Access, 9, pp. 142815–142826, 2021.
https://doi.org/10.1109/ACCESS.2021.3119614

[16] Marugán, A. P., Márquez, F. P. G., Perez, J. M. P., Ruiz-Hernández, D. "A survey of artificial neural network in wind energy systems", Applied Energy, 228, pp. 1822–1836, 2018.
https://doi.org/10.1016/j.apenergy.2018.07.084

[17] Sampaio, G. S., de Aguiar Vallim Filho, A. R., da Silva, L. S., da Silva, L. A. "Prediction of motor failure time using an artificial neural network", Sensors, 19(19), 4342, 2019.
https://doi.org/10.3390/s19194342

[18] Karboua, D., Belgacem, T., Khan, Z. H., Kellal, C. "Robust performance comparison of PMSM for flight control applications in more electric aircraft", PLoS One, 18(7), e0283541, 2023.
https://doi.org/10.1371/journal.pone.0283541

[19] Karimi, M. H., Rostami, M. A., Zamani, H. "Continuous control set model predictive control for the optimal current control of permanent magnet synchronous motors", Control Engineering Practice, 138, 105590, 2023.
https://doi.org/10.1016/j.conengprac.2023.105590

[20] Okada, T., Yamamoto, T., Doi, T., Koiwai, K., Yamashita, K. "Database-driven model predictive control system for online adaptation of an autonomous excavator to environmental conditions", Control Engineering Practice, 145, 105843, 2024.
https://doi.org/10.1016/j.conengprac.2024.105843

[21] Wang, F., Ke, D., Yu, X., Huang, D. "Enhanced predictive model based deadbeat control for PMSM drives using exponential extended state observer", IEEE Transactions on Industrial Electronics, 693, pp. 2357–2369, 2022.
https://doi.org/10.1109/TIE.2021.3065622

[22] Brandić, I., Pezo, L., Bilandžija, N., Peter, A., Šurić, J., Voća, N. "Artificial neural network as a tool for estimation of the higher heating value of miscanthus based on ultimate analysis", Mathematics, 10(20), 3732, 2022.
https://doi.org/10.3390/math10203732

[23] Jain, A., Singh, J., Kumar, S., Florin-Emilian, T., Traian Candin, M. Chithaluru, P. "Improved recurrent neural network schema for validating digital signatures in VANET", Mathematics, 1020, 3895, 2022.
https://doi.org/10.3390/math10203895

[24] Kommula, B. N., Kota, V. R. "An effective sustainable control of brushless DC motor using firefly algorithm – Artificial neural network based FOPID controller", Sustainable Energy Technologies Assessments, 52(B), 102097, 2022.
https://doi.org/10.1016/j.seta.2022.102097

[25] The Mathworks, Inc. "MATLAB (R2021b)", [computer program] Available at: https://www.mathworks.com/products/new_products/release2021b.html [Accessed: 26 April 2024]